JOC The Journal of Organic Chemistry

Featured Article

pubs.acs.org/joc

pH-Dependent Equilibrium between 5-Guanidinohydantoin and Iminoallantoin Affects Nucleotide Insertion Opposite the DNA Lesion

Judy Zhu,[†] Aaron M. Fleming,[†] Anita M. Orendt,[†,‡] and Cynthia J. Burrows*[,†]

[†]Department of Chemistry, University of Utah, 315 South 1400 East, Salt Lake City, Utah 84112-0850, United States

[‡]Center for High Performance Computing, University of Utah, Salt Lake City, Utah 84112-0190, United States

Supporting Information

ABSTRACT: Four-electron oxidation of 2′-deoxyguanosine (dG) yields 5-guanidinohydantoin (dGh) as a product. Previously, we hypothesized that dGh could isomerize to iminoallantoin (dIa) via a mechanism similar to the isomerization of allantoin. The isomerization reaction was monitored by HPLC and found to be pH dependent with a transition pH = 10.1 in which dGh was favored at low pH and dIa was favored at high pH. The structures for these isomers were confirmed by UV−vis, MS, and ^{1}H and ^{13}C NMR. Additionally, the UV−vis and NMR experimental results are supported by density functional theory calculations. A mechanism is proposed to support the pH dependency of the isomerization reaction. Next, we noted the hydantoin ring of dGh mimics thymine, while the iminohydantoin ring of dIa mimics cytosine; consequently, a dGh/dIa site was synthesized in a DNA template strand, and standing start primer extension studies were conducted with Klenow fragment exo^{-}. The dATP/dGTP insertion ratio opposite the dGh/dIa site as a function of pH was evaluated from pH 6.5−9.0. At pH 6.5, only dATP was inserted, but as the pH increased to 9.0, the amount of dGTP insertion steadily increased. This observation supports dGh to dIa isomerization in DNA with a transition pH of ∼8.2.

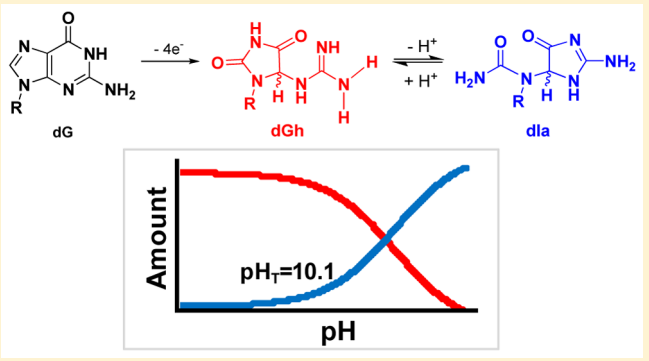

INTRODUCTION

Genomic and mitochondrial DNA are subject to damage or modification from replication errors, hydrolysis, alkylation, and oxidative stress.[1−4] Oxidation of DNA is particularly deleterious because the damaged sites can lead to long pauses in replication or transcription, as well as cause mutations when they are bypassed.[5,6] The heterocyclic base in 2′-deoxyguanosine (dG, E = 1.3 V vs NHE, pH 7) is the most labile toward oxidation because it has the lowest redox potential.[7] In vitro oxidations of dG have identified numerous products, some of which have been observed in vivo.[1,8−11] Mutation profiles for some of the dG oxidation products have been established, identifying them as possible cellular mutagens.[6,12] Moreover, oxidative stress and mutations at dG in the human genome are characteristic of chronic inflammation, a hallmark for a number of driver and passenger mutations in cancers,[13,14] and are observed in many neurological diseases.[15] Determination of the source of these mutations is vital for the development of preventative medicine to stall or prevent diseases resulting from oxidative stress or inflammation.

There exist many candidate dG oxidation products that have the potential to cause mutations. A key member in this product list is the two-electron oxidized species 8-oxo-7,8-dihydro-2′-deoxyguanosine (dOG, Scheme 1).[1,16−19] Quantification of dOG in cells is routinely monitored to assay the extent of oxidative stress.[16,17,20] Even though dOG is a stable compound, it has a low redox potential (E = 0.7 V vs NHE, pH 7)[21] compared to dG, rendering it ∼10^{6} times more susceptible to oxidation. Oxidation of dOG consistently yields the diastereomers of spiroiminodihydantoin-2′-deoxyribonucleoside (dSp) and 5-guanidinohydantoin-2′-deoxyribonucleoside (dGh, Scheme 1) in high yield.[22−28] These hydantoins have been observed in chromate stressed prokaryotes,[11] and eukaryotic cells with chronic inflammation show a dose response in the hydantoin concentrations.[9] The yields of dSp and dGh show a strong dependency on the reaction context and pH, in which dSp is observed in nucleoside reactions at pH > 5.8, single-stranded DNA at pH > 7.0, or G-quadruplex contexts, while high yields of dGh are observed in nucleoside reactions at pH < 5.8, single-stranded DNA at pH < 7.0, or double-stranded DNA contexts.[23,26,29−31] Because cellular pH can span from 6.4 (diabetic cells) to 8.0 (mitochondria), this will affect the ratio of dSp and dGh formation in a cell.[32] Determination of each product's potential mutation profile in vitro is an essential first step for addressing these phenomena in the biological context.

Mutations resulting from dOG are characterized as dG → dT transversions that are nicely illustrated by the Janus-faced base pairing properties of dOG to pair with dCTP on the Watson−

Received: September 16, 2015
Published: November 19, 2015

DOI: 10.1021/acs.joc.5b02180
J. Org. Chem. 2016, 81, 351−359

Scheme 1. Oxidation Pathways of dG Leading to dOG, the Diastereotopic dSp or dGh Lesions, a Seven-Membered Ring Product (1) Observed during Oxidations in Organic Solvents, as Well as Isomerization of dGh to Its Constitutional Isomer dIa Compared to the Analogous Isomerization of Allantoin

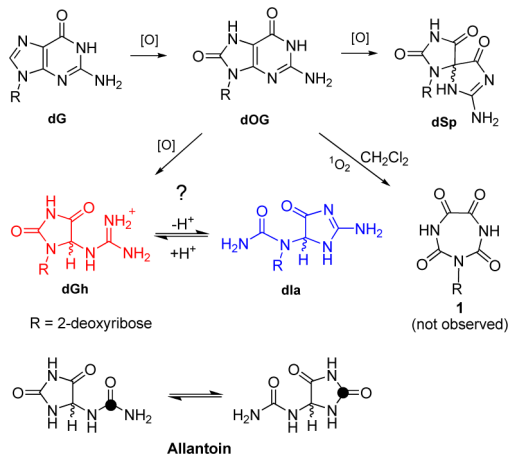

Crick and dATP on the Hoogsteen face.[33] Knockouts of the repair glycosylases for dOG in cells led to an increase in the amount of dG → dT transversions, supporting dOG as the source of these mutations.[34] Experiments to delineate the mutation profiles for the hydantoins in *E. coli* have provided a wealth of data that are less clear than studies with dOG. The dSp diastereomers induce more dG → dC than dG → dT transversion mutations, with strong stereochemical and sequence-context dependency.[6,35,36] Molecular dynamics simulations have provided initial clues to the stereochemical dependency and possible base-pairing rules to explain mutations at dSp sites.[37] High-resolution structures to support the base-pairing simulations currently do not exist. Mutations observed for the dGh diastereomers are established, but structural parameters for them do not completely explain the results.[6,35,36] The dGh isomers consistently induce more dG → dC than dG → dT transversion mutations, and the profiles show a sequence-context dependency.[6,35,36] Line structures support dGh base paring with dATP because the hydantoin ring of dGh has a similar H-bonding pattern as thymine. Two crystal structures with a template (*R*)-dGh and an incoming dATP in the active site of the RB69 DNA polymerase did not show the expected H-bonding between these two bases.[38,39] Structures for (*S*)-dGh have not been obtained. A possible base pair between dGh and dGTP was proposed to be an inverted wobble.[39] In the present work, we propose and provide initial support for an alternative hypothesis to possibly explain the dG → dC transversion mutations observed at dGh sites.

The dGh base architecture has the potential to isomerize, on the basis of an analogy to a similar compound allantoin, an oxidation product of uric acid. Previous studies identified that allantoin can isomerize between two constitutional isomers that differ in the ring atoms (Scheme 1).[40−43] By analogy to allantoin, dGh can isomerize to iminoallantoin-2′-deoxynucleoside (dIa, Scheme 1).[23] In the present study, we determined that a pH-dependent equilibrium exists between dGh and dIa in the nucleoside context with a transition pH = 10.1. The present studies add support for the dGh to dIa equilibrium that was proposed earlier in our laboratory[23] and build off of NMR studies at pH 4.0 and 7.0 that did not observe dIa.[24] The equilibrium is further evaluated in the duplex context by monitoring the pH-dependent insertion of nucleotides opposite the lesion site. This experiment is based on the H-bonding similarity of the hydantoin ring in dGh with thymine to direct dATP insertion and the similarity between the iminoallantoin ring of dIa and cytosine to direct dGTP insertion. The pH-dependent insertion studies found dATP to be the only nucleotide inserted at pH 6.5, and as the pH increased more dGTP insertion was observed. These results provide evidence that the dG → dT transversion mutations may result from dGh, while the dG → dC transversion mutations may result from dIa.[6,35]

RESULTS AND DISCUSSION

A method for synthesizing and purifying the dGh nucleoside on a large scale was developed by adapting literature methods.[24] After HPLC purification under acidic conditions (pH 4.0), the identity of dGh was confirmed by LC-ESI$^+$-MS and ^{1}H and ^{13}C NMR (see below). Next, aliquots of dGh were incubated for 24 h at 22 °C under a range of pH conditions from 4.0−12.5. The samples were analyzed with a Hypercarb HPLC column that readily resolves hydrophilic species while monitoring the elution profile at 240 nm. At pH 4.0, a peak eluting at 5 min was observed (Figure 1A). On the basis of previous studies, this peak was identified as the coeluting dGh diastereomers.[44] Identical results were observed at pH 5.0. Starting at pH 6.0, in addition to the dGh peaks at 5 min, a small set of peaks at 25 min appeared in the chromatogram. Analysis of the samples at

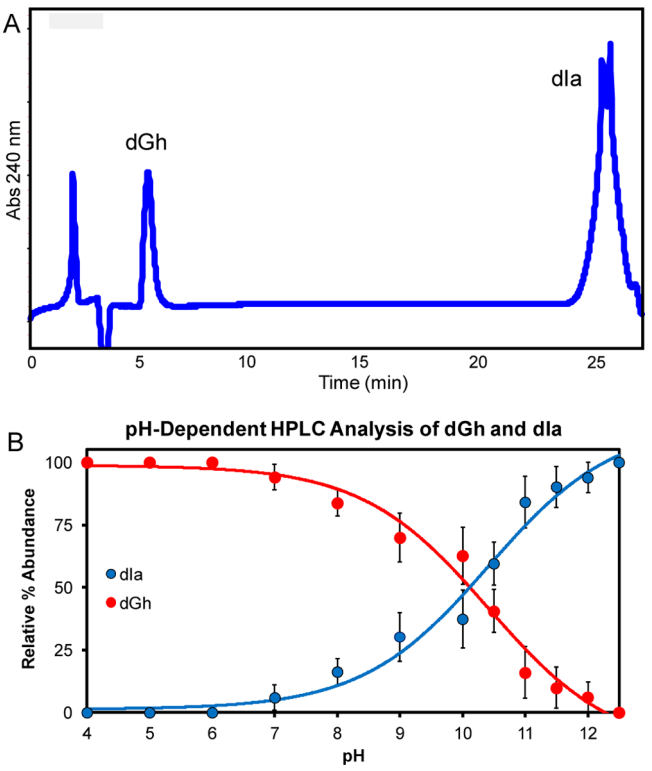

Figure 1. Analysis of the pH-dependent equilibrium between dGh and dIa via HPLC analysis. (A) Sample Hypercarb HPLC trace showing the elution profile for dGh and dIa after incubation at pH 11.5. (B) Plot of the pH-dependent HPLC analysis of dGh and dIa. Relative abundances of the nucleosides were quantified by integrating the area under the elution peaks and normalization by the computed extinction coefficient of each compound at 240 nm.

DOI: 10.1021/acs.joc.5b02180
J. Org. Chem. 2016, 81, 351−359

pH 7.0 to 12.5 identified a trend: as the pH increased, the peak area for the dGh diastereomers decreased while the area for the two peaks at 25 min increased. Analysis of a pH 8.0 sample by LC-ESI$^+$-MS indicated that all four peaks had the same mass calculated for dGh (calculated = 274.3, experimental = 274.1; Figure S1). To further confirm these sets of peaks had the same molecular formula (i.e., constitutional isomers), they were HPLC purified and submitted for HRMS analysis. The analysis identified masses of 296.0980 for the peak with a 5 min retention time and 296.0979 for the peak with a 25 min retention time, both of which were consistent with the mass 296.0971 calculated for the dGh and dIa molecular formula $C_9H_{15}N_5O_5Na$ (i.e., the $[M + Na]^+$ species detected; Figure S2). Confirmation that these peaks have the same molecular formula rules out the seven-membered ring product (**1**) observed by singlet oxygen oxidation of dOG characterized in the Foote laboratory as one of the products (Scheme 1).[45] The seven-membered ring product (**1**) has the same mass as dGh/dIa but with a different molecular formula.

The UV−vis spectrum for the peak at 5 min (dGh) had a λ_{max} = 200 nm with a small shoulder at λ = 220 nm that tailed off to 250 nm, while the peak that eluted at 25 min (dIa) had a λ_{max} = 205 nm that tailed off to 250 nm with no shoulder at 220 nm (Figures S3 and S4). Reproduction of these UV−vis features for dGh (5 min peaks) and dIa (25 min peaks) was achieved by TD-DFT calculations with implicit and explicit solvation included, following a method we previously outlined (Figure 2).[46] For these calculations, the tautomeric form of dGh from the crystal structures was used that was recently reconfirmed by DFT calculations.[38,39,47] The tautomeric form of dIa was mapped by geometric optimization DFT calculations that found the lowest energy structure has an iminohydantoin ring with an N=C double bond conjugated to the carbonyl (Scheme 1 and Figures S3 and S4). Note that these calculations were conducted with a methyl group replacing the ribose to maintain the tautomeric forms. The UV−vis results provided additional support for characterization of dGh and dIa (Figure 2A ,B).

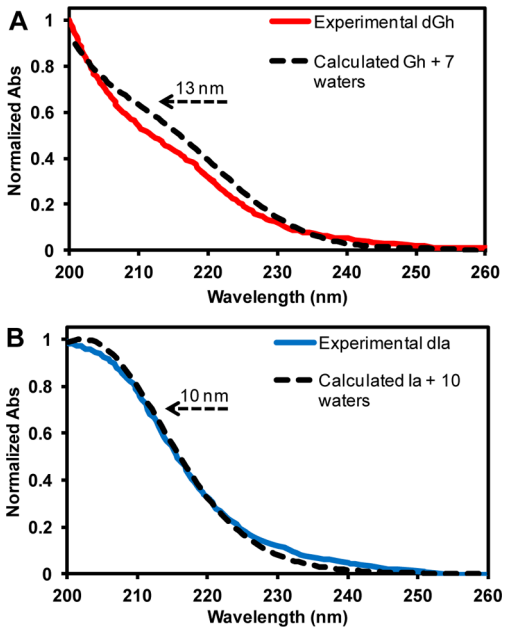

Figure 2. Experimental vs calculated UV−vis spectra for dGh and dIa. The experimental spectra were recorded on the nucleosides during HPLC separation. (A) Comparison of dGh to the TD-DFT simulated UV−vis spectra for Gh with the ribosyl group replaced with a methyl and the addition of seven explicit waters. The theoretical spectrum was blue-shifted by 13 nm to match the experimental spectrum (shown by the dashed arrow). (B) Comparison of dIa to the TD-DFT simulated UV−vis spectrum for Ia with the ribosyl group replaced with a methyl and the addition of 10 explicit waters. The theoretical spectrum was blue-shifted by 10 nm to match the experimental spectrum (shown by the dashed arrow). Details of these calculations are described in the text.

To determine the pH-dependent changes in dGh and dIa from the HPLC injections, their extinction coefficients needed to be determined. A sample of chromatographically pure dIa was not obtainable because dGh was always present up to pH 12.5, after which the compound began to decompose via glycosidic bond hydrolysis; therefore, TD-DFT calculations were conducted to determine the relative extinction coefficients. The values obtained for dGh and dIa were 1800 and 1500 $L \cdot mol^{-1} \cdot cm^{-1}$ at 240 nm, values derived from the computed spectra not normalized in Figure S4, allowing analysis of the pH-dependent HPLC data. A plot of the normalized HPLC peak areas vs pH from 4.0 to 12.5 found dGh to decrease with pH and dIa to increase with pH giving an inflection point at pH 10.1 (Figure 1B). To demonstrate that an equilibrium exists between the two sets of peaks, the new peaks eluting at 25 min appearing at high pH were collected, incubated at pH 4.0, and then reinjected on the HPLC. This study found the 25 min peaks no longer exist and the peaks eluting at 5 min reappeared. The complete interconversion between the isomers occurs after ∼8 h. Next, NMR studies were conducted to establish the structures of dGh and dIa.

To further confirm if dGh was present at low pH and dIa was present at high pH, ^{1}H and ^{13}C NMR spectra were recorded at pH 6.0 and 10.5. Additionally, the diastereomers of dGh were previously shown to interconvert through an enolization reaction on a time scale that prevents their individual study,[24] and a similar isomerization reaction likely occurs with dIa (Figure 3A). Thus, the dGh and dIa diastereomers cannot be individually studied. At pH 6.0, the ^{1}H NMR spectrum showed signals consistent with a set of diastereomers in solution[24] because all observable peaks were doubled and closely spaced (Figures S5 and S6). Furthermore, enolization of the C5 carbonyl causes exchange of the C4 proton with D_2O, preventing its observation. The ^{13}C NMR spectrum also displayed doubling of all the peaks with peak-to-peak distances of 0.1−0.5 ppm (Figure S7). Next, the ^{13}C chemical shifts were compared to those for each diastereomer of dGh and dIa nucleosides determined computationally. The DFT simulations utilized the B3LYP functional and the 6-311G basis set with implicit solvation of water using the PCM model (Figure S11). The calculations identified the *S* diastereomer of dGh and dIa to give consistently more downfield chemical shifts (0.1−1.0 ppm) for analogous proton and carbon atoms relative to the *R* diastereomer. Comparisons between experimental and theoretical values always compared the most downfield experimental shifts with the *S* diastereomer and the most upfield experimental shifts with the *R* diastereomer for each set of closely spaced signals. In Figure 3, plots of Δppm between experimental and theoretical values were constructed (i.e., Δppm = experimental−theoretical). In a previous study from our laboratory,[24] a ^{13}C NMR was conducted on Gh with a triacylated ribosyl group in which C7 was ^{13}C labeled and showed a chemical shift of ∼155 ppm.[24] In the present study

DOI: 10.1021/acs.joc.5b02180
J. Org. Chem. 2016, 81, 351−359

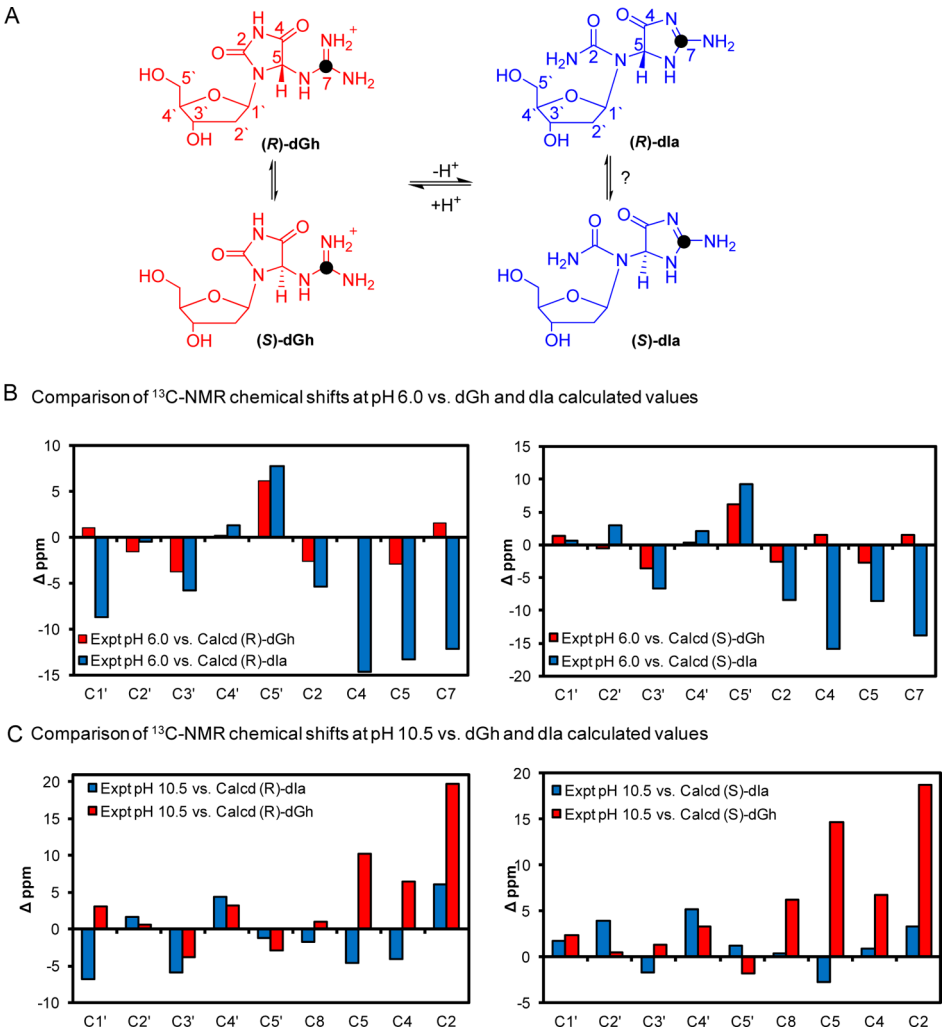

Figure 3. Comparison of ^{13}C NMR chemical shifts experimentally determined at pH 6.0 and 10.5 vs computed values for dGh and dIa. (A) Scheme to illustrate the interconversion between the diastereomers of dGh or dIa and the numbering for both compounds. (B) The Δppm observed for each carbon atom when the pH 6.0 experimental values were compared to the dGh and dIa theoretical values obtained by DFT calculations as described in the text. (C) The Δppm observed for each carbon atom when the pH 10.5 experimental values were compared to the dGh and dIa theoretical values. Comparisons to the *R* diastereomers are on the left and those to the *S* diastereomers are on the right.

Scheme 2. Proposed Mechanism for the pH-Dependent Interconversion between the dGh and dIa Constitutional Isomers (A) and Related Heterocycles (B, C)

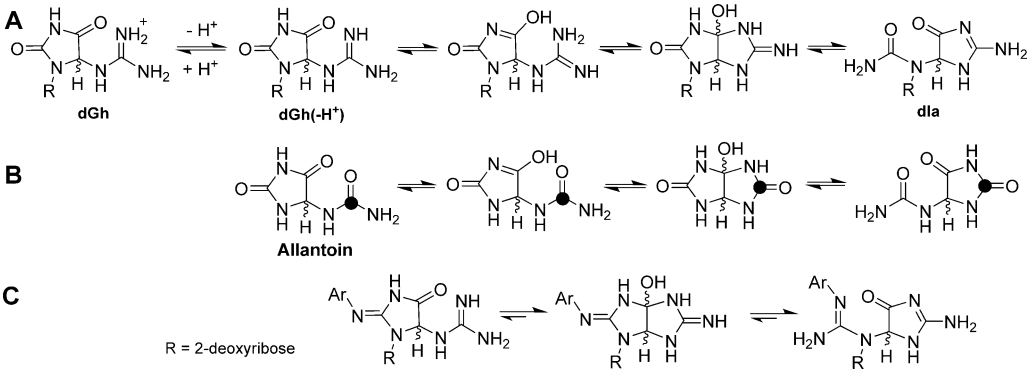

with dGh, C7 has a chemical shift of 156.5 ppm that helped guide our assignments. When experimental ^{13}C values recorded at pH 6.0 were compared to computed values for dGh and dIa, the closest match was observed with the dGh calculated values (Figure 3B blue). All Δppm were <5.0 ppm for the dGh comparisons (Figure 3B blue). In contrast, comparisons to dIa computed values gave Δppm values up to 15 ppm. The largest differences were observed for comparisons with the carbon atoms of the heterocyclic ring, an expected result (Figure 3B red). This observation, in tandem with comparison to our

DOI: 10.1021/acs.joc.5b02180
J. Org. Chem. 2016, 81, 351−359

previous results,[24] support the dGh diastereomers as the constitutional isomers at pH 6.0 that elute from the Hypercarb column at 5 min. Analysis of the individual diastereomers was not conducted because they readily interconvert through an enolization reaction.[24]

In the second NMR study, the sample was incubated at pH 10.5 for 24 h at 22 °C leading to new peaks. In the ^{1}H spectrum, the peak splitting was consistent with four species in solution, two diastereomers of dGh and two diastereomers of dIa (Figures S8 and S9). This observation is also consistent with our HPLC analysis (Figure 1B). The ^{13}C NMR spectrum at pH 10.5 also indicated a mixture of diastereomers for dGh and dIa (Figure S10). Difference plots were then constructed with the new ^{13}C peaks (i.e., the dIa signals) and the theoretical values determined by DFT calculations for dGh and dIa. This comparison showed that the new peaks were more similar to dIa than dGh (Figure 3C). For example, the differences observed for the heterocyclic carbons were <5 ppm for comparisons made to dIa (Figure 3C red), while comparisons made to dGh theoretical values could be nearly 20 ppm different (Figure 3C blue). Again, comparisons to the sugar carbons were much less different for dGh and dIa theoretical values. These comparison support dIa as the other isomer in solution with dGh at pH 10.5; further, this observation is consistent with the HPLC results (Figure 1B). NMR studies were not conducted at pH values >10.5 due to concern about instability of the glycosidic bond leading to free bases in solution that would complicate the results.[48]

The interconversion between dGh and dIa isomers is best explained by a multistep equilibrium reaction mechanism (Scheme 2A). Further, this isomerization is expected to follow the same pathway as reported for allantoin, which has been the topic of many studies over the years (Scheme 2B).[40−43] On the basis of the pH dependency observed for the dGh to dIa equilibrium, we propose the first equilibrium involves deprotonation of the guanidinium group (Scheme 1A). The pK_a for this proton transaction is ∼10.1 on the basis of our results (Figure 1B). Theoretical calculations placed the pK_a for this group at pH 9.6,[49] generally in agreement with the experimental results reported here. Upon deprotonation, the guanidine group attacks C4; however, because of the unfavorable attack trajectory at C4, this must only occur when tautomerized, a point previously made by Abblard et al. for allantoin interconversion (Scheme 2B).[43] This yields a strained bicyclic intermediate that rather quickly decays, because spectroscopic evidence for its presence was not observed. The decay pathway yields dIa at high pH. The equilibrium preference for the double bonds is proposed based on the close comparison between the ^{13}C NMR signals with those derived from DFT simulations (Figures 4B, 4C, and S11). Analogies to the present results can also be made to those observed for 8-arylamine adducts to dG from the Johnson laboratory, in which an allantoin-like structure was proposed (Scheme 2C).[50]

To further support our hypothesis, we conducted studies in the DNA context. Initial attempts to evaluate this isomerization reaction were conducted by synthesizing dGh in a single-stranded oligodeoxynucleotide (ODN) with the sequence 5′-CGT TAX GGC GCA ACT GGA AA-3′ (X = dGh/dIa) by literature methods.[51] The lesion-containing strand was then incubated at different pH values (5.0−9.0) similar to the nucleoside studies and then analyzed by ion-exchange HPLC. However, the peak distribution in the HPLC did not change as

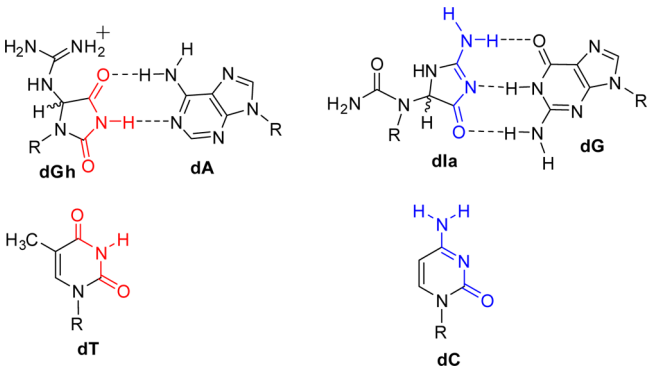

Figure 4. Line drawings for the dGh·dA and dIa·dG base pairs to illustrate the proposed mimickry of dT by dGh and dC by dIa.

a function of pH (Figure S12), leading us to an alternative approach for reaction analysis. Polymerase insertion assays were conducted to determine if the choice of dNTP insertion opposite the dGh/dIa site would change as a function of pH. This experiment was proposed based on the hypothesis that the hydantoin ring of dGh mimics thymine and would preferentially favor dATP insertion opposite at low pH (Figure 4); in contrast, the iminohydantoin ring of dIa is a cytosine mimic and would favor dGTP insertion opposite the lesion as the pH increased (Figure 4). A site-specific lesion was synthesized by literature methods in the same 20-mer sequence described above.[51] The primer sequence was a 5′-^{32}P radiolabeled 14-mer strand (5′-TT TCC AGT TGC GCC-3′), and after annealing, the duplex was incubated at different pH conditions (pH 6.5−9.0) for 24 h at 22 °C. These studies were conducted as standing start polymerase insertion assays, meaning the first site at which the polymerase inserts a dNTP was opposite the lesion. The polymerase selected for this study was Klenow fragment exo$^-$ (Kf exo$^-$) because it has high activity across a broad range of pH conditions.[52] Studies were conducted with one dNTP at a time. On the basis of previous studies,[53] dTTP should not be inserted opposite the lesion site; therefore, a dA nucleotide was placed 3′ to the dGh/dIa to ensure that only one dNTP was inserted. By only allowing one nucleotide extension, quantification of dNTP selection (i.e., base pairing) vs pH was evaluated.

The initial analysis was conducted at pH 8.0, a value near the optimum for Kf exo$^-$, as reported by the manufacturer. All four dNTPs were studied, and as expected, neither dCTP nor dTTP was inserted opposite the lesion (Figure S13), and they are therefore not provided in Figure 5A. At pH 6.5, the nucleotide incorporation opposite the lesion was exclusively dATP (Figure 5A). This exclusivity changed for reactions conducted at pH ≥ 7.0, in which both dATP and dGTP were found to be inserted (Figure 5A). Starting at pH 7.0, the amount of dGTP incorporation increased as the pH increased, reaching a nearly 1:1 ratio of dATP vs dGTP insertion between pH 8.0 and 8.5 (∼8.2). Polymerase insertions at pH 9.0 gave slightly more dGTP insertion than dATP, and studies were not conducted above this pH due to instability of the ODN duplex (Figure S8).

Before interpretation of these results with dGh/dIa in templating ODN strands, a control study that varied pH while monitoring dNTP insertion opposite a lesion that does not change structure with pH was conducted. The lesion selected was dSp (Scheme 1), and it was synthesized at the same site as dGh via literature protocols.[53] This control experiment will rule

DOI: 10.1021/acs.joc.5b02180
J. Org. Chem. 2016, 81, 351−359

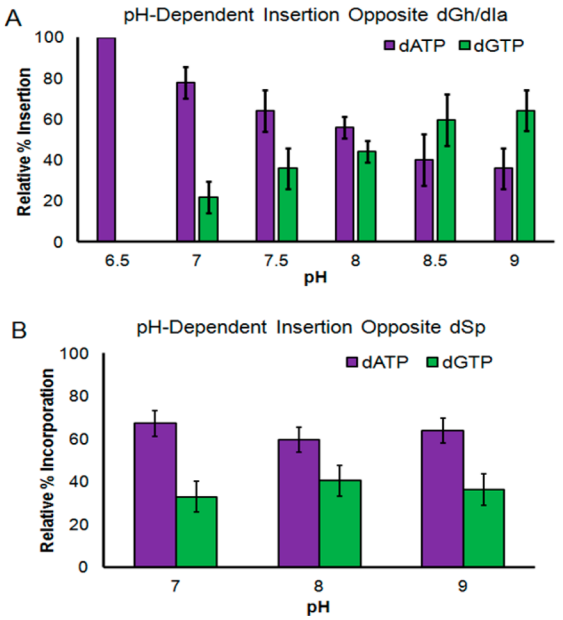

Figure 5. pH-dependent insertion of dATP or dGTP opposite a dGh/dIa site or dSp site via the DNA polymerase Kf exo$^-$. (A) Plot for the pH-dependent insertion opposite dGh/dIa. (B) Plots for the pH-dependent insertion opposite dSp.

out any changes in the polymerase that might occur as the pH was altered. As the pH varied from 7.0 to 9.0, the ratio of dATP to dGTP insertion remained the same at nearly a 1.5:1.0 ratio, respectively (Figure 5B). This observation confirms the properties of Kf exo$^-$ remain the same across the pH range studied. Thus, the pH-dependent trend observed for dNTP insertion opposite dGh/dIa results from changes in lesion structure.

By varying the pH and monitoring the preference for dNTP selection opposite the dGh/dIa site, we were able to evaluate if this isomerization reaction occurs in ODN strands. The polymerization data support the interconversion between the dGh and dIa in ODNs (Scheme 2A). Specifically, at pH 6.5 only dATP was incorporated, indicating the presence of dGh, a mimic of dT. While starting at pH 7.0 and above, dGTP was also inserted, and the amount inserted increased with increasing pH. This observation supports the dGh to dIa isomerization reaction in DNA. This trend continued to pH 9.0, but could not be conducted at higher pH due to duplex instability past this point. In light of this limitation, the polymerase results support the pK_a for the guanidinium group on dGh to be around ∼8.2 in duplex ODNs, due to deprotonation of this group unmasking the nucleophile allowing the isomerization reaction (Scheme 2A). If Kf exo$^-$ is reading out dGh or dIa in the template strand, the duplex context causes a reduction of almost 2 pH units for the pK_a of the guanidinium group. This large difference may reflect the ability of dIa to be more easily accommodated in the ODN context relative to dGh. Though, this claim cannot be confirmed until high resolution structures are obtained. Further, this provides initial support that dIa can exist in DNA at pH ≥ 7.0.

In the last study, the ability to extend the dGh/dIa site when either dATP or dGTP was inserted opposite was evaluated. The template sequence allowed mixing dATP or dGTP with dTTP to address this question because the next base in the template was an A (template = 5′-CGT TAX GGC GCA ACT GGA AA-3′ (X = dGh/dIa). When dGTP and dTTP were mixed, the ability to extend was observed by a band two nucleotides longer than the starting primer. When dATP and dTTP were mixed, the ability to extend was determined by a primer length four nucleotides longer, because the template has two Ts after the A, so reactions containing dATP yielded longer products. Polymerase extension reactions at pH 8.0 where the amount of dGh and dIa would be nearly equal found the amount of bypassed product to be the same when dATP and dGTP were present. This observation demonstrates that Kf exo$^-$ can extend past the dA·dGh and dG·dIa base pairs with nearly equal efficiency (Figure S13).

CONCLUSIONS

Our laboratory hypothesized a number of years ago that dGh could isomerize to its constitutional isomer dIa,[23] although a subsequent NMR study at pH 4.0 and 7.0 came to the conclusion that dIa did not exist.[24] In the present work, the pH was extended to 12.5, providing a transition pH = 10.1 for the interconversion between dGh and dIa nucleosides (Figure 1B). The dGh and dIa structures and transition are based on HPLC, UV−vis, MS, and ^{1}H and ^{13}C NMR studies (Figures 1−3). The UV−vis and NMR results were interpreted with the guidance of DFT calculations. Mechanistically, the interconversion between dGh and dIa is proposed to follow a similar pathway as for the isomerization of allantoin, a uric acid oxidation product.[40−43] We propose a multistep reaction pathway to describe the pH-dependent equilibrium between dGh and dIa (Scheme 2A). The key first step involves deprotonation of the guanidinium group of dGh to unmask the nucleophile, allowing attack of this group at the C4 carbon. This attack yields a strained intermediate that rapidly decomposes to dIa. Thus, dGh dominates at pH < 10.1 and dIa at pH > 10.1. Further, the experimental transition pH closely reflects the calculated pK_a (9.6) for the guanidinium group derived from DFT simulations by the Schlegel laboratory.[49]

Lastly, dGh/dIa was synthesized in an ODN template and polymerase bypass studies were conducted to elucidate the possible base-pairing properties at this site. Because the hydantoin ring of dGh is a mimic of thymine, it should preferentially base pair with dATP, while the iminohydantoin ring of dIa is a mimic of cytosine, and should preferentially base pair with dGTP (Figure 4). Single-nucleotide insertion studies with dATP or dGTP vs pH were conducted and found a pH-dependent trend that followed these predictions: at low pH, dATP was the preferred nucleotide inserted, and as the pH was increased, dGTP insertion increased. The pH-transition point for dATP vs dGTP insertion was ∼8.2 (Figure 5A). Further, bypass was equally proficient when either dATP or dGTP was installed. These results add initial support for dGh isomerizing to dIa in the ODN context. High-resolution structural studies will need to be conducted in a pH-dependent fashion to confirm this observation.

The isomerization between dGh and dIa provides an additional example of C-substituted hydantoins bearing nucleophilic groups undergoing isomerization between two ring architectures, another example being isomerization of allantion.[40−43] In the case of dGh/dIa, the isomerization is pH dependent and regulated by the protonation state of the guanidinium group on dGh.

One goal of the present work was to better understand why in vivo mutagenesis studies observed high amounts of dG → dC transversion mutations at dGh sites.[6,35] Base pairing

DOI: 10.1021/acs.joc.5b02180
J. Org. Chem. 2016, 81, 351−359

between dGh and dGTP is not immediately clear; in contrast, if dGh isomerizes to dIa, base pairing with dGTP can be more easily explained (Figure 4). The polymerase extension results in the sequence context 5′-AXG-3′ (X = dGh/dIa) confirm the dATP vs dGTP insertion ratio is highly impacted by pH. Though, to obtain >50% insertion preference of dGTP, the pH must be > ∼8.2. The sequence context may play a role in nucleotide insertion, but this should have a minor impact on the dGh to dIa isomerization. Biomolecules in the cellular context reside near neutrality and only deviate from this pH under extreme circumstances. Further, these extremes tend to be acidotic such as observed in diabetes,[54] rheumatoid arthoritis,[55] or muscular dystrophy,[56] for example, and will always favor a shift in the equilibrium to dGh, therefore, leading to more dATP insertion and dG → dT mutations.[57] On the other hand, alkalosis is observed in mitochondria (pH 8.0),[32] and tumor cells can also have intracellular alkalosis.[58] These conditions would favor a shift in the equilibrium to more dIa, but dGh would still dominate (Figures 1B and 5A). When dIa is present, dGTP insertion would yield dG → dC mutations. These chemical arguments neglect the impact that cellular proteins and other features of the cell may play on the dGh to dIa isomerization. Additionally, there is yet any evaluation of the impact of pH on DNA repair,[59] and it is possible that dGh vs dIa have different repair efficiencies leading to a bias in the mutations observed at these sites.

The final implication of these results resides in detection of dGh/dIa from cellular sources. Processing of genomic, and likely in the future, transcriptomic samples is conducted under conditions that terminate in alkaline hydrolysis (pH ∼ 8) of the nuclease-liberated monophosphates.[9,60,61] Because the retention times for dGh (∼5 min) and dIa (∼25 min) are so dramatically different on the Hypercarb column, if complete analysis of the LC run is not conducted, quantification of dIa will not be achieved. By not quantifying dIa, the results of such studies would report values for dGh that could be off by >20%. Due to the low concentrations of these compounds in cells to start with, an incomplete analysis could dramatically impact the interpretations of such studies.

EXPERIMENTAL SECTION

Synthesis of dGh Nucleoside. Preparation of dGh was achieved by following a literature method.[24] Briefly, dG (1 mM) in a 100 mL solution placed in a watch glass was reacted with the photooxidant Rose Bengal (5 μM) in 10 mM NaOAc buffer (pH 4, 22 °C). The reaction was initiated by irradiating the sample with a 350 nm light (300 W light bulb suspended ∼8 cm above the reaction) for 1 h. The Rose Bengal was removed by passing the reaction mixture through a solid-phase extraction cartridge (Sep-Pak SPE, Waters Corp) using H_2O as the extraction solvent. Purification of dGh nucleoside was conducted using a two-column purification method. On the first column, unreacted dG was separated from the dGh by passing the eluent through a reversed-phase HPLC column (100 × 4.6 mm, 5 μm) running the following solvents: A = ddH_2O, B = CH_3CN with a flow rate of 1 mL/min while monitoring the absorbance at 240 nm. The method was initially isocratic with 1% B for 3 min followed by a linear increase to 65% B over 10 min. The dGh was collected in the void volume of this HPLC run. The void volume from the previous run was lyophilized to dryness and reinjected on a second HPLC column. The dried void volume containing the dGh was purified using a Hypercarb HPLC column (150 × 4.6 mm, 5 μm). The resolving solvents included A = ddH_2O with 0.1% acetic acid, and B = MeOH with a flow rate of 1 mL/min while monitoring the absorbance at 240 nm. The method was initiated with an isocratic gradient of 0% B for the first 20 min followed by a linear gradient in B to 75% over 20 min. The dGh diastereomer retention time was 5 min. The yield for dGh was 3% based on the amount of material recovered after oxidation and purification. The identity of the dGh nucleoside was initially confirmed by LC-MS (ESI) m/z $[M + H]^+$ calcd mass = 274.3, experimental mass = 274.1.

dGh and dIa Nucleoside Studies. The purified dGh nucleoside was subjected to conditions of varying pH (pH 4.0, 5.0, 6.0, 7.0, 8.0, 9.0, 10.0, 10.5, 11.0, 11.5, 12.0, and 12.5). The buffers included 20 mM NaOAc at low pH values (pH 4.0 and 5.0), 20 mM NaP_i at the higher pH values (pH 6.0, 7.0, and 8.0), and 20 mM borate at the highest pH values (9.0, 10.0, 10.5, 11.0, 11.5, 12.0, and 12.5). A sample of nucleoside was placed at each pH and incubated at 22 °C for 24 h followed by analysis via the Hypercarb HPLC column using the method previously described. The dIa isomers appeared when the pH ≥ 7.0, and have the same mass as dGh (experimental $[M + H]^+$ = 274.1, calculated $[M + H]^+$ = 274.1).

The relative amounts of dGh and dIa were quantified based on integration of the peak areas determined by their absorbance at 240 nm. Obtaining pure dIa was not achievable because even at pH 12.5 some dGh remained, and going higher in pH caused decomposition of the nucleoside. Therefore, to determine the relative extinction coefficients for dGh and dIa, time-dependent density functional theory (TD-DFT) calculations using the Gaussian09 software package were utilized.[62] Calculations were conducted on the Gh and Ia free bases bearing a methyl group at the nitrogen on which the 2-deoxyribose would be attached, and the calculations were conducted with implicit and explicit solvation as previously outlined by our laboratory.[46] The tautomeric form of Gh was based on previous X-ray crystal structures,[38,39] while the tautomeric form of Ia was determined by energy minimization calculations as described below (Figure S3). The explicitly solvated structures for Gh required 7 waters where as for Ia 10 waters were required. The structures were optimized with the B3LYP functional and 6-311G basis set while implicitly defining the solvent as water with the polarizable continuum model (PCM).[63−68] The UV−vis spectra were determined from the explicitly solvated optimized structures via TD-DFT calculations using the M06-2X[69] functional and the 6-311G++(2d,2p) basis set while implicitly defining the solvent as water with the PCM model. This approach allowed reproduction of the UV−vis spectra, and determination of the $\varepsilon_{240\ nm}$ ($L{\cdot}mol^{-1}{\cdot}cm^{-1}$) values were determined to be 1800 for dGh and 1500 for dIa. These values were used for normalization of the HPLC peak areas to determine the relative amounts of each isomer. All UV−vis spectra were visualized using GaussView v 5.0 software.[70]

dGh and dIa NMR Studies. Purified dGh/dIa (∼2 mg) was dissolved in 350 μL of D_2O at either pH 6.0 (50 mM NaP_i) or 10.5 (50 mM sodium borate). After the samples had incubated at the desired pH for 24 h at 22 °C, ^{1}H- and ^{13}C NMR experiments were performed. The ^{1}H NMR (500 MHz, D_2O) (pH 6.0) δ 5.89 (dd, J = 6.48 + 6.42 Hz), 5.78 (dd, J = 2.88 + 7.95 Hz), 4.21 (m), 3.79 (m), 3.75 (m), 3.61 (d, J = 4.02 Hz), 3.58 (d, J = 4.09 Hz), 3.55 (m), 3.47 (d, J = 6.11 Hz), 3.45 (d, J = 6.18 Hz), 2.28 (m), 2.20 (m), 2.10 (b); (pH 10.) δ 5.89 (dd, J = 5.99 + 6.05 Hz), 5.77 (m), 4.28 (m), 4.20 (m), 3.76 (m), 3.73 (m), 3.67 (d, J = 4.16 Hz), 3.65 (d, J = 4.03 Hz), 3.53 (m), 3.50 (d, J = 6.00 Hz), 3.45 (d, J = 6.00 Hz), 2.21 (m), 2.12 (m), 2.03 (m); ^{13}C NMR (125 MHz, D_2O) (pH 6.0) δ 178.1, 176.7, 163.8, 156.5, 153.0, 85.2, 84.9, 82.0, 81.9, 71.1, 71.0, 70.8, 70.7, 61.9, 61.6, 36.1, 35.1; (pH 10.5) δ 191.2, 186.7, 172.4, 171.2, 170.2, 161.9, 156.5, 156.3, 86.9, 86.3, 84.9, 84.6, 76.1, 71.3, 71.2, 70.9, 70.8, 70.3, 62.0, 61.8, 37.3, 37.2. The experimental chemical shifts were compared to those obtained for dGh and dIa via DFT calculations. The dGh and dIa structures were optimized with the B3LYP functional and the 6-311G basis set with implicit definition of water via the PCM model. The optimized structures were obtained on the nucleosides of each isomer; further, the preferred rotamers were elucidated by rotational scans about the glycosidic bond and C5,N6 dihedral angles for dGh as well as the glycosidic bond and N1,C2 dihedral angles for dIa. The theoretical chemical shifts were obtained on the optimized structures with the gauge including atomic orbitals (GIAO)[71] with the B3LYP functional running the 6-311++G basis set with implicit definition of

DOI: 10.1021/acs.joc.5b02180
J. Org. Chem. 2016, 81, 351−359

water via the PCM model. The calculated chemical shielding values were converted to chemical shifts using regression analysis.[72]

Synthesis of dGh and dIa in ODNs. ODNs were synthesized via standard solid-phase synthesis with the dOG phosphoramidite (Glen Research, Sterling, VA) at the desired site of modification in the sequence 5′-CGT TAX GGC GCA ACT GGA AA-3′ where X is dOG. The dGh modification was synthesized by taking 1 nmol of the dOG-containing strand in ddH_2O and adding Na_2IrCl_6 (12 nmol, 12 equiv) in a 100-μL reaction. The dGh-containing ODNs were purified using an ion-exchange HPLC column running the following solvents: A= 10% CH_3CN in ddH_2O, B = 1.5 mM NaOAc in 10% CH_3CN (pH 7) with a flow rate of 1 mL/min and monitoring the absorbance at 260 nm. The method was initiated at 15% B followed by a linear gradient to 100% B over 30 min. The dGh ODN elutes as two peaks. The identity of the purified ODN containing dGh or dIa was verified by MALDI-MS ($[M + H]^+$), calcd = 6198.1, expt = 6198.5.

Nucleotide Triphosphate Insertion Studies. The duplex used for the base-pairing studies was made by annealing 125 nM primer (5′-TT TCC AGT TGC GCC-3′) with 156 nM of the previously described damage-containing template to obtain 125 nM duplex in buffers with different pH values. For the lower pH (6.5 and 7.0) conditions, the buffer was 50 mM HEPES with 50 mM NaCl, 5 mM $MgCl_2$, and 1 mM DTT. While at the higher pH (7.5, 8.0, 8.5, and 9.0) conditions, the buffer was 50 mM Tris with 50 mM NaCl, 5 mM $MgCl_2$, and 1 mM DTT. The primer strand was labeled with ^{32}P via literature protocols[30] and 20000 cpm was added to each reaction mixture. The duplexes were annealed in a 90 °C heat bath for 5 min before slowly cooling to room temperature over ∼3 h.

For the polymerase insertion reaction, 20 μL of the annealed duplex, 1 μL of Kf exo$^-$ (New England Biolabs, 0.2 units/μL), and 0.5 μL of dNTP (from a 500 μM stock solution) was added to a 25 μL reaction to obtain a 100 nM duplex, 10 μM dNTP solution with 0.2 units of polymerase. The four canonical dNTPs were studied individually. The Kf exo$^-$ was added last to commence the reaction that progressed at 37 °C for 30 min. The reactions were quenched by adding gel loading dye (95% DMF, 0.025% bromophenol blue, and 0.025% xylene cyanol) and heating the samples at 90 °C for 15 min. The reactions were analyzed on a 20% denaturing polyacrylamide gel (PAGE) that was electrophoresed for 3 h at 45 W. After electrophoresis, the gel was placed in a phosphor screen and exposed for 24 h. The screen was imaged by storage phosphor autoradiography and the band intensities were quantified using ImageQuant software.

■ ASSOCIATED CONTENT

Supporting Information

The Supporting Information is available free of charge on the ACS Publications website at DOI: 10.1021/acs.joc.5b02180.

LC-ESI$^+$-MS, HRMS, ^1H and ^{13}C NMR, and PAGE analysis for the polymerase studies, dihedral scan energies, and coordinates for DFT-optimized structures (PDF)

■ AUTHOR INFORMATION

Corresponding Author

*Phone: (801) 585-7290. E-mail: burrows@chem.utah.edu.

Notes

The authors declare no competing financial interest.

■ ACKNOWLEDGMENTS

This work was supported by a National Institutes of Health grant (R01 CA090689). The oligonucleotides were provided by the DNA/Peptide core facility at the University of Utah that is supported in part by the NCI Cancer Center Support grant (P30 CA042014). A.M.O. is supported in part by a National Science Foundation grant (1341935). Computational resources are gratefully acknowledged from the Center for High Performance Computing at the University of Utah. We thank Dr. Peter Flynn (University of Utah) for help with the NMR experiments. J.Z. was supported in part by the College of Science ACCESS Program and Undergraduate Research Opportunities Program (UROP) at the University of Utah. We thank Abby Wilson for preparation of the cover art.

■ REFERENCES

(1) Cadet, J.; Wagner, J. R.; Shafirovich, V.; Geacintov, N. E. *Int. J. Radiat. Biol.* **2014**, *90*, 423−432.
(2) Gates, K. *Chem. Res. Toxicol.* **2009**, *22*, 1747−1760.
(3) Schermerhorn, K. M.; Delaney, S. *Acc. Chem. Res.* **2014**, *47*, 1238−1246.
(4) Kunkel, T. A. *Curr. Opin. Chem. Biol.* **2011**, *15*, 620−626.
(5) Saxowsky, T. T.; Doetsch, P. W. *Chem. Rev.* **2006**, *106*, 474−488.
(6) Henderson, P. T.; Delaney, J. C.; Muller, J. G.; Neeley, W. L.; Tannenbaum, S. R.; Burrows, C. J.; Essigmann, J. M. *Biochemistry* **2003**, *42*, 9257−9262.
(7) Steenken, S.; Jovanovic, S. V. *J. Am. Chem. Soc.* **1997**, *119*, 617−618.
(8) Neeley, W. L.; Essigmann, J. M. *Chem. Res. Toxicol.* **2006**, *19*, 491−505.
(9) Mangerich, A.; Knutson, C. G.; Parry, N. M.; Muthupalani, S.; Ye, W.; Prestwich, E.; Cui, L.; McFaline, J. L.; Mobley, M.; Ge, Z.; Taghizadeh, K.; Wishnok, J. S.; Wogan, G. N.; Fox, J. G.; Tannenbaum, S. R.; Dedon, P. C. *Proc. Natl. Acad. Sci. U. S. A.* **2012**, *109*, E1820−E1829.
(10) Matter, B.; Malejka-Giganti, D.; Csallany, A. S.; Tretyakova, N. *Nucleic Acids Res.* **2006**, *34*, 5449−5460.
(11) Hailer, M. K.; Slade, P. G.; Martin, B. D.; Sugden, K. D. *Chem. Res. Toxicol.* **2005**, *18*, 1378−1383.
(12) Grollman, A. P.; Moriya, M. *Trends Genet.* **1993**, *9*, 246−249.
(13) Pfeifer, G.; Besaratinia, A. *Hum. Genet.* **2009**, *125*, 493−506.
(14) Greenman, C.; Stephens, P.; Smith, R.; Dalgliesh, G. L.; Hunter, C.; Bignell, G.; Davies, H.; Teague, J.; Butler, A.; Stevens, C.; Edkins, S.; O'Meara, S.; Vastrik, I.; Schmidt, E. E.; Avis, T.; Barthorpe, S.; Bhamra, G.; Buck, G.; Choudhury, B.; Clements, J.; Cole, J.; Dicks, E.; Forbes, S.; Gray, K.; Halliday, K.; Harrison, R.; Hills, K.; Hinton, J.; Jenkinson, A.; Jones, D.; Menzies, A.; Mironenko, T.; Perry, J.; Raine, K.; Richardson, D.; Shepherd, R.; Small, A.; Tofts, C.; Varian, J.; Webb, T.; West, S.; Widaa, S.; Yates, A.; Cahill, D. P.; Louis, D. N.; Goldstraw, P.; Nicholson, A. G.; Brasseur, F.; Looijenga, L.; Weber, B. L.; Chiew, Y. E.; DeFazio, A.; Greaves, M. F.; Green, A. R.; Campbell, P.; Birney, E.; Easton, D. F.; Chenevix-Trench, G.; Tan, M. H.; Khoo, S. K.; Teh, B. T.; Yuen, S. T.; Leung, S. Y.; Wooster, R.; Futreal, P. A.; Stratton, M. R. *Nature* **2007**, *446*, 153−158.
(15) Heinzen, E. L.; Neale, B. M.; Traynelis, S. F.; Allen, A. S.; Goldstein, D. B. *Annu. Rev. Neurosci.* **2015**, *38*, 47−68.
(16) Gedik, C. M.; Collins, A. *FASEB J.* **2005**, *19*, 82−84.
(17) Delaney, S.; Jarem, D. A.; Volle, C. B.; Yennie, C. J. *Free Radical Res.* **2012**, *46*, 420−441.
(18) Pratviel, G.; Meunier, B. *Chem. - Eur. J.* **2006**, *12*, 6018−6030.
(19) Gimisis, T.; Cismas, C. *Eur. J. Org. Chem.* **2006**, *2006*, 1351−1378.
(20) Burrows, C. J.; Muller, J. G. *Chem. Rev.* **1998**, *98*, 1109−1152.
(21) Steenken, S.; Jovanovic, S. V.; Bietti, M.; Bernhard, K. *J. Am. Chem. Soc.* **2000**, *122*, 2373−2374.
(22) Luo, W.; Muller, J. G.; Rachlin, E. M.; Burrows, C. J. *Org. Lett.* **2000**, *2*, 613−616.
(23) Luo, W.; Muller, J. G.; Rachlin, E. M.; Burrows, C. J. *Chem. Res. Toxicol.* **2001**, *14*, 927−938.
(24) Ye, Y.; Muller, J. G.; Luo, W.; Mayne, C. L.; Shallop, A. J.; Jones, R. A.; Burrows, C. J. *J. Am. Chem. Soc.* **2003**, *125*, 13926−13927.
(25) Niles, J. C.; Wishnok, J. S.; Tannenbaum, S. R. *Org. Lett.* **2001**, *3*, 963−966.
(26) Niles, J. C.; Wishnok, J. S.; Tannenbaum, S. R. *Chem. Res. Toxicol.* **2004**, *17*, 1510−1519.

DOI: 10.1021/acs.joc.5b02180
J. Org. Chem. 2016, 81, 351−359

(27) Crean, C.; Geacintov, N. E.; Shafirovich, V. *Angew. Chem., Int. Ed.* **2005**, *44*, 5057−5060.
(28) Sugden, K. D.; Campo, C. K.; Martin, B. D. *Chem. Res. Toxicol.* **2001**, *14*, 1315−1322.
(29) Fleming, A. M.; Muller, J. G.; Dlouhy, A. C.; Burrows, C. J. *J. Am. Chem. Soc.* **2012**, *134*, 15091−15102.
(30) Fleming, A. M.; Burrows, C. J. *Chem. Res. Toxicol.* **2013**, *26*, 593−607.
(31) Gremaud, J. N.; Martin, B. D.; Sugden, K. D. *Chem. Res. Toxicol.* **2010**, *23*, 379−385.
(32) Casey, J. R.; Grinstein, S.; Orlowski, J. *Nat. Rev. Mol. Cell Biol.* **2010**, *11*, 50−61.
(33) Shibutani, S.; Takeshita, M.; Grollman, A. P. *Nature* **1991**, *349*, 431−434.
(34) Ohno, M.; Sakumi, K.; Fukumura, R.; Furuichi, M.; Iwasaki, Y.; Hokama, M.; Ikemura, T.; Tsuzuki, T.; Gondo, Y.; Nakabeppu, Y. *Sci. Rep.* **2014**, *4*, 4689.
(35) Neeley, W. L.; Delaney, S.; Alekseyev, Y. O.; Jarosz, D. F.; Delaney, J. C.; Walker, G. C.; Essigmann, J. M. *J. Biol. Chem.* **2007**, *282*, 12741−12748.
(36) Delaney, S.; Delaney, J. C.; Essigmann, J. M. *Chem. Res. Toxicol.* **2007**, *20*, 1718−1729.
(37) Jia, L.; Shafirovich, V.; Shapiro, R.; Geacintov, N. E.; Broyde, S. *Biochemistry* **2005**, *44*, 13342−13353.
(38) Aller, P.; Ye, Y.; Wallace, S. S.; Burrows, C. J.; Doublie, S. *Biochemistry* **2010**, *49*, 2502−2509.
(39) Beckman, J.; Wang, M.; Blaha, G.; Wang, J.; Konigsberg, W. H. *Biochemistry* **2010**, *49*, 8554−8563.
(40) Poje, M.; Sokolic-Maravic, L. *Tetrahedron* **1986**, *42*, 747−751.
(41) Poje, M.; Sokolic-Maravic, L. *Tetrahedron* **1988**, *44*, 6723−6728.
(42) Kahn, K.; Serfozo, P.; Tipton, P. A. *J. Am. Chem. Soc.* **1997**, *119*, 5435−5442.
(43) Abblard, J.; Meynaud, A.; Definod, G. *Bull. Soc. Chim. Fr.* **1971**, *159*, 942−946.
(44) Fleming, A. M.; Muller, J. G.; Ji, I.; Burrows, C. J. *Org. Biomol. Chem.* **2011**, *9*, 3338−3348.
(45) Sheu, C.; Foote, C. S. *J. Am. Chem. Soc.* **1995**, *117*, 474−477.
(46) Fleming, A. M.; Orendt, A. M.; He, Y.; Zhu, J.; Dukor, R. K.; Burrows, C. J. *J. Am. Chem. Soc.* **2013**, *135*, 18191−18204.
(47) Jena, N. R.; Gaur, V.; Mishra, P. C. *Phys. Chem. Chem. Phys.* **2015**, *17*, 18111−18120.
(48) Fleming, A. M.; Alshykhly, O.; Zhu, J.; Muller, J. G.; Burrows, C. J. *Chem. Res. Toxicol.* **2015**, *28*, 1292−1300.
(49) Verdolino, V.; Cammi, R.; Munk, B. H.; Schlegel, H. B. *J. Phys. Chem. B* **2008**, *112*, 16860−16873.
(50) Shibutani, S.; Gentles, R. G.; Iden, C. R.; Johnson, F. *J. Am. Chem. Soc.* **1990**, *112*, 5667−5668.
(51) Zhou, J.; Liu, M.; Fleming, A. M.; Burrows, C. J.; Wallace, S. S. *J. Biol. Chem.* **2013**, *288*, 27263−27272.
(52) Spratt, T. E.; Levy, D. E. *Nucleic Acids Res.* **1997**, *25*, 3354−3361.
(53) Kornyushyna, O.; Berges, A. M.; Muller, J. G.; Burrows, C. J. *Biochemistry* **2002**, *41*, 15304−15314.
(54) Khandoudi, N.; Bernard, M.; Cozzone, P.; Feuvray, D. *Diabetes* **1995**, *44*, 196−202.
(55) Collins, J. A.; Moots, R. J.; Winstanley, R.; Clegg, P. D.; Milner, P. I. *Osteoarthr. Cartilage* **2013**, *21*, 1790−1798.
(56) Lo Cascio, C. M.; Latshang, T. D.; Kohler, M.; Fehr, T.; Bloch, K. E. *Respiration* **2014**, *87*, 499−503.
(57) Kornyushyna, O.; Burrows, C. J. *Biochemistry* **2003**, *42*, 13008−13018.
(58) Chiche, J.; Brahimi-Horn, M. C.; Pouysségur, J. *J. Cell. Mol. Med.* **2010**, *14*, 771−794.
(59) Zhao, X.; Krishnamurthy, N.; Burrows, C. J.; David, S. S. *Biochemistry* **2010**, *49*, 1658−1666.
(60) Su, D.; Chan, C. T.; Gu, C.; Lim, K. S.; Chionh, Y. H.; McBee, M. E.; Russell, B. S.; Babu, I. R.; Begley, T. J.; Dedon, P. C. *Nat. Protoc.* **2014**, *9*, 828−841.
(61) Taghizadeh, K.; McFaline, J. L.; Pang, B.; Sullivan, M.; Dong, M.; Plummer, E.; Dedon, P. C. *Nat. Protoc.* **2008**, *3*, 1287−1298.
(62) Frisch, G. W.; et al. *Gaussian 09, revision C.01*; Gaussian, Inc.: Wallingford, CT, 2010.
(63) Becke, A. D. *J. Chem. Phys.* **1993**, *98*, 5648−5652.
(64) Lee, C.; Yang, W.; Parr, R. G. *Phys. Rev. B: Condens. Matter Mater. Phys.* **1988**, *37*, 785−789.
(65) Krishnan, R.; Binkley, J. S.; Seeger, R.; Pople, J. A. *J. Chem. Phys.* **1980**, *72*, 650−654.
(66) Frisch, M. J.; Pople, J. A.; Binkley, J. S. *J. Chem. Phys.* **1984**, *80*, 3265−3269.
(67) Scalmani, G.; Frisch, M. J. *J. Chem. Phys.* **2010**, *132*, 114110.
(68) Tomasi, J.; Mennucci, B.; Cammi, R. *Chem. Rev.* **2005**, *105*, 2999−3093.
(69) Zhao, Y.; Truhlar, D. *Theor. Chem. Acc.* **2008**, *120*, 215−241.
(70) Dennington, R.; Keith, T.; Millam, J. *GaussView, Version 5*; Semichem, Inc.: Shawnedd Mission, KS, 2009.
(71) Cheeseman, J. R.; Trucks, G. W.; Keith, T. A.; Frisch, M. J. *J. Chem. Phys.* **1996**, *104*, 5497−5509.
(72) Barich, D. H.; Orendt, A. M.; Pugmire, R. J.; Grant, D. M. *J. Phys. Chem. A* **2000**, *104*, 8290−8295.

DOI: 10.1021/acs.joc.5b02180
J. Org. Chem. 2016, 81, 351−359